The Astrophysical Journal, 664:1121–1129, 2007 August 1
© 2007. The American Astronomical Society. All rights reserved. Printed in U.S.A.

THE LONG-PERIOD, MASSIVE BINARIES HD 37366 AND HD 54662: POTENTIAL TARGETS FOR LONG-BASELINE OPTICAL INTERFEROMETRY[1]

T. S. Boyajian,[2] D. R. Gies,[2] J. P. Dunn, C. D. Farrington, E. D. Grundstrom,[2] W. Huang,[3]
M. V. McSwain,[2,4,5] S. J. Williams,[2] and D. W. Wingert[2]
Center for High Angular Resolution Astronomy and Department of Physics and Astronomy, Georgia State University, Atlanta, GA 30302-4106;
tabetha@chara.gsu.edu, gies@chara.gsu.edu, dunn@chara.gsu.edu, farrington@chara.gsu.edu, erika@chara.gsu.edu,
wenjin@astro.caltech.edu, mcswain@astro.yale.edu, swilliams@chara.gsu.edu, wingert@chara.gsu.edu

A. W. Fullerton
Space Telescope Science Institute, Baltimore, MD 21218; fullerton@stsci.edu

and

C. T. Bolton
David Dunlap Observatory, University of Toronto, Richmond Hill, ON L4C 4Y6, Canada; bolton@astro.utoronto.ca
Received 2006 December 12; accepted 2007 April 22

ABSTRACT

We present the results from an optical spectroscopic analysis of the massive stars HD 37366 and HD 54662. We find that HD 37366 is a double-lined spectroscopic binary with a period of 31.8187 ± 0.0004 days, and HD 54662 is also a double-lined binary with a much longer period of 557.8 ± 0.3 days. The primary of HD 37366 is classified as O9.5 V, and it contributes approximately two-thirds of the optical flux. The less luminous secondary is a broad-lined, early B-type main-sequence star. Tomographic reconstruction of the individual spectra of HD 37366 reveals absorption lines present in each component, enabling us to constrain the nature of the secondary and physical characteristics of both stars. Tomographic reconstruction was not possible for HD 54662; however, we do present mean spectra from our observations that show that the secondary component is approximately half as bright as the primary. The observed spectral energy distributions (SEDs) were fit with model SEDs and galactic reddening curves to determine the angular sizes of the stars. By assuming radii appropriate for their classifications, we determine distance ranges of 1.4–1.9 and 1.2–1.5 kpc for HD 37366 and HD 54662, respectively.

Subject headings: binaries: spectroscopic — stars: early-type — stars: individual (HD 37366, HD 54662)

1. INTRODUCTION

There remains considerable uncertainty about the masses of the most massive stars because of the relatively small number of known binary systems for which accurate masses can be determined (Gies 2003). Spectroscopic measurements alone yield mass functions dependent on the unknown orbital inclination, and the determination of inclination requires either the good fortune of finding eclipsing binaries or the angular resolution of the orbit on the sky. The angular semimajor axis of a binary (in units of milliarcseconds) is given by

$$a(\mathrm{mas}) = 0.28\,\frac{[P/(10\ \mathrm{days})]^{2/3}[M_{\mathrm{total}}/(30\ M_{\odot})]^{1/3}}{[d/(1\ \mathrm{kpc})]}, \quad (1)$$

where P is the orbital period, M_{total} is the combined mass of the stars, and d is the distance. The denominators of each unit give typical values for these parameters among OB binaries, and the leading coefficient of 0.28 mas indicates that most massive systems are probably too closely separated for direct resolution with optical long-baseline interferometers, where the limits are currently above 1 mas. The key objective here is to find double-lined spectroscopic binaries with long orbital periods. Such binaries are difficult to detect because their orbital semiamplitudes are small, the component lines are often blended, and a long-term observational program is required to obtain adequate phase coverage. The best candidates for direct resolution are 15 Mon ($P \approx$ 25 yr; Gies et al. 1997), HD 15558 ($P = 442$ days; Garmany & Massey 1981; De Becker et al. 2006), and HD 193322 ($P =$ 311 days; McKibben et al. 1998).

Here we report on new orbits for two such long-period massive binaries, HD 37366 and HD 54662. The star HD 37366 (BD +30 968, HIP 26611, O9.5 V; Walborn 1973) is a member of the Aur OB1 association at a distance of approximately 1.3 kpc (Humphreys 1978). This association has many bright early-type giants and supergiants, but HD 37366 has the earliest spectral type among the member stars that still reside on the main sequence. The *Hipparcos* mission (Perryman et al. 1997) detected a visual companion to HD 37366 with $\Delta H_p = 3.5$, a separation of 0.58″, and a period of approximately 1300 yr (Mason et al. 1998). The brighter component of these two stars ($H_p = 7.7$) is a radial velocity variable (Petrie & Pearce 1961; Young 1942), and it is known to show asymmetry in its spectral lines (Grigsby et al. 1992). Observations with the *International Ultraviolet Explorer* (*IUE*) confirm that the spectrum displays double lines (Stickland & Lloyd 2001).

[1] Based on observations obtained at the Canada-France-Hawaii Telescope (CFHT), which is operated by the National Research Council of Canada, the Institut National des Sciences de l'Univers of the Centre National de la Recherche Scientifique of France, and the University of Hawaii.

[2] Visiting Astronomer, Kitt Peak National Observatory, National Optical Astronomy Observatory.

[3] Current address: Department of Astronomy, California Institute of Technology, Pasadena, CA 91125.

[4] Current address: Astronomy Department, Yale University, New Haven, CT 06520-8101.

[5] NSF Astronomy and Astrophysics Postdoctoral Fellow.

The second target, HD 54662 (BD −10 1892, HIP 34536, LS 197, O6.5 V; Walborn 1972), is also the brightest and earliest member of its resident association, CMa OB1, at a distance of 1.3 kpc (Humphreys 1978). Radial velocity measurements for HD 54662 extend back many decades (Plaskett 1924; Conti et al. 1977; Garmany et al. 1980), and these display only modest variability. However, Fullerton (1990) noted the presence of blue extensions to the spectral lines that probably indicate the presence of a companion in a long-period orbit. The scatter in the *IUE* velocities also indicates that the star is a binary (Stickland & Lloyd 2001).

Here we present an analysis of the radial velocities and spectra of both stars from spectroscopic observations that we have obtained over the past few years (§ 2). We discuss each system's orbital velocity solution (§ 3) and the spectral and physical properties of each component star in these binaries (§§ 4 and 5). We conclude with a consideration of the prospects for the angular resolution of the orbits using optical long-baseline interferometry (§ 6).

2. OBSERVATIONS

We observed HD 37366 and HD 54662 with the Kitt Peak National Observatory (KPNO) 0.9 m coudé feed telescope during two separate observing runs in 2000 October and December. The spectra were made using the long collimator, grating B (in second order with order sorting filter OG 550), camera 5, and the F3KB CCD, a Ford Aerospace 3072 × 1024 device with 15 μm square pixels. The setup yielded a resolving power of $R = \lambda/\delta\lambda = 9500$, with a spectral coverage of 6440–7105 Å. Exposure times were usually 10 minutes or less, and we generally obtained two spectra (taken a few hours apart) each night. For HD 37366, we made two more red spectral observations in 2004 October using a similar arrangement but with a different detector, the T2KB CCD (2048 × 2048 24 μm square pixels). In 2006 October, both HD 37366 and HD 54662 were observed in the red region again using this same instrumental setup. We also observed the rapidly rotating A-type star, ζ Aql, which we used for removal of atmospheric water vapor and O_2 bands. Each set of observations was accompanied by numerous bias, flat-field, and Th-Ar comparison lamp calibration frames.

We also obtained a small set of blue spectra of these targets. For HD 37366, the first group of four spectra were made in 2005 October with the KPNO 2.1 m telescope and GoldCam spectrometer. We used the No. 47 grating in second order, recording the spectral region from 4050 to 4950 Å with a resolving power of $R = \lambda/\delta\lambda \approx 3000$. Then in 2005 November and 2006 October we obtained higher resolution observations in the blue with the KPNO coudé feed 0.9 m telescope. HD 37366 was observed on both occasions, whereas HD 54662 was only included during the 2006 observing run. We used grating A in second order with order sorting filter 4-96, camera 5, and the T2KB CCD. This setup gave us a resolving power of $R = \lambda/\delta\lambda \approx 12{,}100$ and a wavelength coverage of 4240–4585 Å.

The spectra were extracted and calibrated using standard routines in IRAF.[6] All the spectra were rectified to a unit continuum by fitting line-free regions. The removal of atmospheric lines from the red spectra was done by creating a library of ζ Aql spectra from each run, removing the broad stellar features from these, and then dividing each target spectrum by the modified atmospheric spectrum that most closely matched the target spectrum in a selected region dominated by atmospheric absorptions. The spectra from each run were then transformed to a common heliocentric wavelength grid.

[6] IRAF is distributed by the National Optical Astronomy Observatory, which is operated by the Association of Universities for Research in Astronomy, Inc., under cooperative agreement with the National Science Foundation.

3. RADIAL VELOCITIES AND ORBITAL ELEMENTS

3.1. *HD 37366*

We measured radial velocities of the high-resolution red spectra collected in 2000 and 2006 using a template fitting scheme (Gies et al. 2002) for the He I λ6678 line. We decided not to measure the other strong lines in this region because the binary components are badly blended in the Hα profile, and the He I λ7065 line was marred by residual features left behind by the telluric cleaning procedure. This radial velocity measurement scheme assigns template spectra that are approximate matches for the primary (hotter and more massive star) and secondary spectra, and then makes a nonlinear least-squares fit of the shifts for each component that best matches the observed line profile. We need to make assumptions at the outset about the temperature, gravity, projected rotational velocity, and flux contribution of each star, but these can be checked after completion of the velocity analysis by studying the properties of tomographically reconstructed spectra of the components (§ 4).

The matching template spectra for the primary and secondary components were constructed from the grid of O-type star model spectra from Lanz & Hubeny (2003) that are based on the line-blanketed, non-LTE, plane-parallel, hydrostatic atmosphere code TLUSTY and the radiative transfer code SYNSPEC (Hubeny 1988; Hubeny & Lanz 1995; Hubeny et al. 1998). We selected the spectrum taken on HJD 2,451,901.92, which shows well-separated, individual components of each star, as a reference to determine the approximate spectral parameters for both stars.

The template fitting procedure also requires preliminary estimates of the primary and secondary stars' radial velocities. We estimated these for each spectrum with well-separated lines using the IRAF `splot` routine and deblend option to fit two Gaussians to each composite profile. We also measured relative radial velocity shifts of the strong interstellar lines in all the spectra referenced to the first spectrum in the stack. We then used these relative shifts in the interstellar lines (which should remain motionless) to make additional small corrections for the wavelength calibrations (all these corrections were <2 km s^{-1}).

The final radial velocities from this template fitting procedure (the majority of the observations) are listed in Table 1 along with the heliocentric Julian date of mid-observation, the corresponding orbital phase, and the residual from the orbital fit (observed minus calculated) for both the primary and the secondary. The typical errors in these velocities are also listed in Table 1. We measure only one line for this data set, so we list the characteristic errors (not individual errors), which are based on the scatter in closely spaced pairs of observations. These errors are 1.3 and 2.2 km s^{-1} for the primary and secondary, respectively.

This template fitting routine was also used in determining radial velocities for the high-resolution blue spectra (collected in 2005 November and 2006 October), using the four lines O II λ4349, He I $\lambda\lambda$4387, 4471, and Mg II λ4481. We followed the same procedure in obtaining the spectral templates and the preliminary radial velocity estimates as described above. Since no strong interstellar features are apparent in this region, no additional radial velocity correction was applied. The line-to-line

TABLE 1
HD 37366 Radial Velocity Measurements

HJD (−2,400,000)	Telescope/Band	Orbital Phase	V_1 (km s^{-1})	σ_1 (km s^{-1})	$(O-C)_1$ (km s^{-1})	V_2 (km s^{-1})	σ_2 (km s^{-1})	$(O-C)_2$ (km s^{-1})
46,821.612	*IUE*/UV	0.303	76.9	5.0	0.7	−57.3	10.0	4.3
46,866.116	*IUE*/UV	0.702	13.2	5.0	−0.5	...	...	...
51,817.934	CF/red	0.327	75.9	1.3	−1.3	−64.5	2.2	−1.5
51,818.938	CF/red	0.358	76.2	1.3	−1.0	−67.1	2.2	−4.1
51,819.929	CF/red	0.389	75.5	1.3	−0.6	−53.2	2.2	8.3
51,820.922	CF/red	0.420	74.7	1.3	0.8	−63.8	2.2	−5.2
51,821.918	CF/red	0.452	71.2	1.3	0.4	−51.9	2.2	2.5
51,822.918	CF/red	0.483	64.1	1.3	−2.7	−49.4	2.2	−0.3
51,823.853	CF/red	0.513	62.2	1.3	−0.1	−38.1	2.2	4.9
51,823.980	CF/red	0.517	60.1	1.3	−1.5	−41.7	2.2	0.4
51,824.881	CF/red	0.545	55.8	1.3	−0.7	−38.8	2.2	−3.6
51,824.997	CF/red	0.549	57.1	1.3	1.3	−36.9	2.2	−2.6
51,830.904	CF/red	0.734	0.2	1.3	−1.1	45.9	2.2	7.4
51,889.881	CF/red	0.588	47.9	1.3	0.5	−26.0	2.2	−3.0
51,890.819	CF/red	0.617	42.0	1.3	2.0	−20.9	2.2	−7.6
51,892.787	CF/red	0.679	20.9	1.3	−0.8	17.9	2.2	6.7
51,893.855	CF/red	0.713	9.6	1.3	−0.2	26.5	2.2	−0.7
51,894.780	CF/red	0.742	−1.6	1.3	0.3	53.6	2.2	10.9
51,894.856	CF/red	0.744	−3.3	1.3	−0.5	47.2	2.2	3.2
51,895.874	CF/red	0.776	−19.6	1.3	−2.4	58.7	2.2	−4.5
51,896.802	CF/red	0.805	−32.7	1.3	−1.0	78.4	2.2	−4.2
51,896.914	CF/red	0.809	−34.6	1.3	−1.0	78.8	2.2	−6.1
51,897.802	CF/red	0.837	−46.9	1.3	1.7	100.7	2.2	−4.4
51,897.910	CF/red	0.840	−51.4	1.3	−0.8	96.0	2.2	−11.6
51,898.811	CF/red	0.868	−66.2	1.3	0.3	128.1	2.2	−0.8
51,898.922	CF/red	0.872	−68.7	1.3	−0.2	133.2	2.2	1.6
51,899.809	CF/red	0.900	−83.5	1.3	−0.1	153.0	2.2	1.7
51,899.915	CF/red	0.903	−84.4	1.3	0.5	154.2	2.2	0.7
51,900.802	CF/red	0.931	−95.5	1.3	0.6	171.8	2.2	3.5
51,900.908	CF/red	0.934	−96.3	1.3	0.7	172.6	2.2	3.1
51,901.788	CF/red	0.962	−99.8	1.3	0.3	173.7	2.2	0.2
51,901.917	CF/red	0.966	−100.5	1.3	−0.7	177.2	2.2	4.1
53,291.928	CF/red	0.651	30.8	2.6	0.2	...	...	...
53,292.984	CF/red	0.684	20.6	0.4	0.6	...	...	...
53,658.997[a]	2.1 m/blue	0.187	52.6	6.7	−0.8	...	...	...
53,659.000[a]	2.1 m/blue	0.187	51.5	1.4	−2.0	...	...	...
53,663.010[a]	2.1 m/blue	0.313	71.6	0.4	−5.0	...	...	...
53,663.989[a]	2.1 m/blue	0.344	89.0	4.2	11.7	...	...	...
53,684.903	CF/blue	0.001	−85.7	1.3	0.8	155.4	4.2	0.1
53,686.902	CF/blue	0.064	−30.1	0.7	0.9	76.3	9.8	−4.9
53,688.846	CF/blue	0.125	21.9	0.9	0.9	13.1	5.2	1.3
54,020.972	CF/red	0.564	51.2	1.8	−1.1	−25.8	2.2	4.1
54,024.926	CF/red	0.688	17.4	2.8	−1.0	13.9	3.4	−1.1
54,030.021	CF/blue	0.848	−56.0	2.0	−0.8	103.2	2.4	−9.3
54,031.999	CF/blue	0.911	−90.1	2.9	−1.7	144.4	3.5	−12.0

[a] Zero weight.

1 σ errors in these V_R measurements are <1 km s^{-1} for the primary and 4–9 km s^{-1} for the secondary (Table 1). These final V_R measurements are also presented in Table 1.

The four observations made in the blue during 2005 October had a much lower resolution, thus making it difficult to apply this method of template fitting. To avoid possible errors from unseen line blending in the two components, we chose to measure only radial velocities of the He II $\lambda\lambda$4541, 4686 lines present, since these lines are found only in the spectrum of the much hotter, primary star (§ 4). We used a parabolic fitting routine to determine the mean velocities of these lines (Table 1). The line-to-line 1 σ errors associated with these measurements are <6 km s^{-1} (Table 1).

The two red observations made in 2004 showed no indication of double-lined profiles. In this case, we measured velocities only for the primary star by parabolic fitting of the line cores of He I $\lambda\lambda$6678, 7065 in order to minimize the influence of the secondary on the line profile. The line-to-line 1 σ error associated with these fits are <2 km s^{-1} (exclusive of blending errors). These velocities are also presented in Table 1.

The final two spectra of HD 37366 were collected and downloaded from the archive of the *IUE* satellite.[7] We measured radial velocities for these two high-dispersion, short-wavelength, prime camera spectra using a cross-correlation method (Penny et al. 1999) with the spectrum of HD 34078 as the reference template. The spectrum was double-lined in the first spectrum, SWP 30165. The errors are approximately 5 km s^{-1} for the

[7] See http://archive.stsci.edu/iue/.

TABLE 2
Orbital Elements for HD 37366

Element (1)	Primary (2)	Secondary (3)	Joint Solution (4)
P (days)	31.8187 ± 0.0004	31.822 ± 0.002	31.8188[a]
T_1 (HJD −2,400,000)	53653.013 ± 0.04	...	53653.02[a]
T_2 (HJD −2,400,000)	...	53653.15 ± 0.19	53653.02[a]
e_1	0.329 ± 0.003	...	0.330[a]
e_2	...	0.35 ± 0.012	0.330[a]
ω_1 (deg)	211.4 ± 0.6	...	211.6[a]
ω_2 (deg)	...	212 ± 2	211.6[a]
K_1 (km s^{-1})	88.6 ± 0.3	...	88.7 ± 0.2
K_2 (km s^{-1})	...	118.4 ± 1.6	117.4 ± 1.2
γ_1 (km s^{-1})	13.3 ± 0.2	...	13.3 ± 0.2
γ_2 (km s^{-1})	...	20.6 ± 1.3	21.6 ± 0.9
$M_1 \sin^3 i$ ($M_\odot$)	13.8 ± 0.3	...	13.9 ± 0.3
$M_2 \sin^3 i$ ($M_\odot$)	...	10.5 ± 0.1	10.42 ± 0.08
$a_1 \sin i$ ($R_\odot$)	52.6 ± 0.2	...	52.62 ± 0.13
$a_2 \sin i$ ($R_\odot$)	...	69.7 ± 1.0	69.7 ± 0.7
σ_1 (km s^{-1})	1.1	...	1.0
σ_2 (km s^{-1})	...	5.3	5.4

[a] Fixed.

primary and 10 km s^{-1} for the secondary. These final velocities are also presented in Table 1.

The radial velocities from all the data sets (six total) span 20 yr with 45 radial velocity measurements for the primary and 38 radial velocity measurements for the secondary (Table 1). We first constructed a power spectrum using all the primary star's radial velocity measurements, being more reliable and plentiful, to identify possible orbital periods for the binary. We used the discrete Fourier transform and CLEAN deconvolution algorithm (Roberts et al. 1987), which shows that the strongest signal occurs near $P = 31.7$ days. We then used this estimate as a starting value for the period in fits of the orbital elements.

We determined the orbital elements of the binary using the nonlinear, least-squares, orbital fitting program from Morbey & Brosterhus (1974). We began with a fit of the primary's velocities that is given in column (2) of Table 2 done with equal weighting except for the low-resolution blue spectra, which have a weight set to zero. This solution has a period of 31.8187 ± 0.0004 days. The independent orbital solution for the secondary has a period of 31.822 ± 0.002 days, given in column (3) of Table 2. Since the independent solutions agree well with each other, we derive a joint solution by fixing the weighted means of the shared orbital parameters (P, T, e, ω) found in the independent solutions for the binary in order to make fits of the systemic velocity, $\gamma_{1,2}$, and the semiamplitude, $K_{1,2}$, for each component (col. [4] of Table 2). In the case of massive binaries, the systemic velocities of the components may not agree exactly because of differences in their expanding atmospheres and/or, in our case, differences in the shapes of the template spectra for the He I λ6678, He II λ6683 blend. The radial velocity curves for the joint solution are plotted together with the observations in Figure 1. We also made similar fits weighting each point by the normalized, inverse square of its associated error; these results matched within errors of those from the equal weighting fits given in Table 2.

3.2. *HD 54662*

We obtained relative radial velocities for the primary (hotter, more massive) star in HD 54662 by cross-correlation with a single spectrum of the star that had good signal-to-noise ratio (S/N) properties. These relative velocities were transformed to an absolute velocity scale by adding the mean velocity measured through parabolic fits to the cores of the absorption lines in this reference spectrum. All the strong lines were included in the cross-correlation measurements, namely, Hα, He I λ6678 + He II λ6683, and He I λ7065. We excluded He II $\lambda\lambda$6527, 6890 because their measurements deviated from the set listed above, as well as compared to each other. We suspect that the residual telluric lines in the spectra, which are very prominent in these regions, are the cause of this disagreement. The velocities for the primary star are presented in Table 3, along with the average velocity and σ (line-to-line) from the C IV $\lambda\lambda$5801, 5812 and He I λ5876 lines presented by Fullerton (1990). We were unable to measure velocities for the secondary star in individual

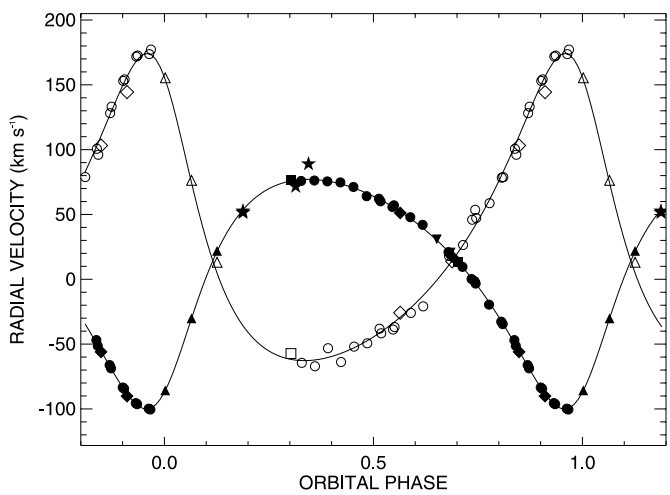

Fig. 1.—Calculated radial velocity curves (*solid lines*) for HD 37366. The primary and secondary stars' measured radial velocities are indicated by circles (2000), inverted triangles (2004 October), stars (2005 October), triangles (2005 November), diamonds (2006 October), and squares (*IUE* 1987). The filled symbols correspond to the primary, and the open symbols correspond to the secondary. The uncertainties in individual measurements are generally smaller than the size of the symbols.

TABLE 3
HD 54662 Primary Radial Velocity Measurements

HJD (−2,400,000)	Telescope/Band	Orbital Phase	V_r (km s^{-1})	σ(line-line) (km s^{-1})	$O-C$ (km s^{-1})
46,426.830	CFHT/yellow	0.191	62.2	2.0	−0.3
46,426.904	CFHT/yellow	0.191	61.3	1.6	−1.1
46,426.980	CFHT/yellow	0.191	61.8	1.6	−0.6
46,427.802	CFHT/yellow	0.192	61.3	1.7	−1.2
46,427.869	CFHT/yellow	0.192	61.6	2.2	−0.9
46,427.925	CFHT/yellow	0.193	61.1	2.0	−1.4
46,427.973	CFHT/yellow	0.193	61.5	1.6	−1.0
46,428.036	CFHT/yellow	0.193	61.6	1.4	−0.9
46,428.132	CFHT/yellow	0.193	62.0	2.1	−0.5
46,428.805	CFHT/yellow	0.194	62.2	2.0	−0.3
46,429.021	CFHT/yellow	0.194	61.4	1.9	−1.2
46,429.814	CFHT/yellow	0.196	61.8	1.7	−0.8
46,429.883	CFHT/yellow	0.196	61.5	2.1	−1.1
46,432.853	CFHT/yellow	0.201	61.4	2.1	−1.3
46,432.897	CFHT/yellow	0.201	60.9	1.4	−1.8
46,432.999	CFHT/yellow	0.202	62.2	2.0	−0.5
46,433.093	CFHT/yellow	0.202	61.2	1.5	−1.6
51,817.967	CF/red	0.855	33.2	0.6	0.0
51,818.962	CF/red	0.857	33.5	2.5	0.4
51,819.962	CF/red	0.859	33.7	1.1	0.7
51,820.990	CF/red	0.860	33.0	2.1	0.1
51,821.968	CF/red	0.862	33.0	0.9	0.2
51,822.941	CF/red	0.864	34.6	3.7	1.9
51,823.957	CF/red	0.866	34.5	3.4	1.8
51,824.903	CF/red	0.867	35.2	1.2	2.6
51,889.990	CF/red	0.984	37.5	2.6	0.7
51,890.923	CF/red	0.986	37.1	1.2	0.0
51,892.899	CF/red	0.989	35.0	2.0	−2.6
51,893.926	CF/red	0.991	37.5	1.9	−0.3
51,894.882	CF/red	0.993	37.5	1.5	−0.6
51,894.956	CF/red	0.993	39.0	2.3	0.9
51,895.934	CF/red	0.995	37.6	1.3	−0.8
51,896.033	CF/red	0.995	39.0	1.6	0.6
51,896.881	CF/red	0.996	39.4	0.6	0.8
51,896.952	CF/red	0.997	37.0	1.6	−1.7
51,897.879	CF/red	0.998	37.9	1.7	−1.0
51,897.943	CF/red	0.998	37.1	1.6	−1.8
51,898.891	CF/red	0.000	39.1	2.5	−0.1
51,898.953	CF/red	0.000	38.3	2.0	−0.9
51,899.885	CF/red	0.002	37.4	0.8	−2.1
51,899.947	CF/red	0.002	38.3	0.5	−1.2
51,900.878	CF/red	0.004	39.0	2.9	−0.8
51,900.940	CF/red	0.004	38.7	3.1	−1.1
51,901.885	CF/red	0.005	39.5	2.9	−0.6
51901.949	CF/red	0.006	39.1	2.8	−1.0
54,020.025	CF/red	0.802	33.9	7.5	−2.5
54,024.964	CF/red	0.811	31.8	5.6	−4.0
54,027.025	CF/blue	0.815	35.8	5.0	0.2
54,028.964	CF/blue	0.819	34.4	6.4	−0.9
54,030.961	CF/blue	0.822	37.4	4.4	2.3
54,032.012	CF/blue	0.824	35.2	4.3	0.2

spectra due to severe line blending with profiles of the primary star (see § 5).

Published velocities for HD 54662 (§ 1) do not show significant variations. Table 3 shows that our measurements change only slightly over our observation period. However, Fullerton (1990) found convincing evidence that this system is a double-lined binary with either a long period or high eccentricity, since he observed a blueshifted secondary component (suspected O7 spectral type) in the profiles of C IV $\lambda\lambda$5801, 5812 and He I λ5876.

Here we present a preliminary orbital solution for the primary component that was determined using our measurements combined with published measurements (Plaskett 1924; Garmany et al. 1980; Fullerton 1990; Stickland & Lloyd 2001) for a total of 67 radial velocities spanning 85 yr. Stickland & Lloyd (2001) proposed a possible period of ≈92 days; however, their orbit was determined excluding selected data points. We reinvestigated the possible period by power-spectrum analysis of all the available data. We examined all the peaks in the CLEANed spectrum using the nonlinear, least-squares, orbital fitting routine,

TABLE 4
PRELIMINARY ORBITAL ELEMENTS FOR HD 54662

Element	Value
P (days)	557.8 ± 0.3
T (HJD −2,400,000)	22333 ± 5
e	0.28 ± 0.04
ω (deg)	238 ± 5
K (km s^{-1})[a]	15.9 ± 0.5
γ (km s^{-1})	49.9 ± 0.6
$f(m)$ ($M_\odot$)[a]	0.20 ± 0.02
$a_1 \sin i$ ($R_\odot$)[a]	168 ± 6
rms (km s^{-1})	3.3

[a] Lower limit due to line blending.

and among the periods limited by the timescales sampled in our two long runs, we find that the best solution occurs at a period of ≈558 days. This confirms the suggestion from Fullerton (1990) that HD 54662 is in fact a long-period binary. Table 4 lists the preliminary orbital elements for HD 54662 assuming equal weighting for all velocities, and this solution is plotted in Figure 2. We show below (§ 5) that these results are affected by line blending, and the derived semiamplitude, for example, is a lower limit to the actual value. It is also possible that the results collected in the literature have systematic differences related to the specific lines and measurement techniques used. These systematic offsets are likely much smaller than the system semiamplitude, and since this system has such a long orbital period, we include all available measurements for this preliminary orbital solution.

4. TOMOGRAPHIC SPECTRAL RECONSTRUCTION AND STELLAR PARAMETERS FOR HD 37366

We used a Doppler tomography algorithm (Bagnuolo et al. 1994) to separate the primary and secondary spectra of HD 37366. We applied tomographic reconstruction to the red spectra collected in 2000 (30 total) and to the high-dispersion blue spectra collected in 2005 and 2006 (five total). Figure 3 shows the reconstructed red spectra for the primary (*top*) and the secondary (*bottom*). The region affected by the atmospheric band from ≈6850 to 7000 Å was set to unity. The secondary spectrum shows the weak lines of O II $\lambda\lambda$6641, 6721 and C II $\lambda\lambda$6578, 6582. These lines are absent in the primary spectrum, which shows instead features such as He II λ6683 that are found in O-type spectra. To determine a monochromatic flux ratio, F_2/F_1, we used the equivalent width of He I λ6678, since it does not change significantly with spectral type for late-O to early-B stars (Conti 1974). These equivalent widths in the primary and secondary reconstructed spectra are equal for a flux ratio of $F_2/F_1 = 0.35 \pm 0.05$.

We fit these reconstructed spectra with the TLUSTY/SYNSPEC model synthetic spectra (see § 3) to estimate the projected rotational velocity $V \sin i$, effective temperature $T_{\rm eff}$, and gravity $\log g$. These values are listed for both components of HD 37366 in Table 5 (where subscript 1 identifies the primary and 2 the secondary). For stars like these, the disappearance of the C II and O II lines and the emergence of the He II and Si IV lines with increasing temperature provide a useful temperature estimate, while the width of the Hα wings is sensitive to the adopted gravity. The $V \sin i$ was measured using a rotational broadening function applied to the model spectra to fit the two He I absorption lines. The red spectra were first used in the determination of these

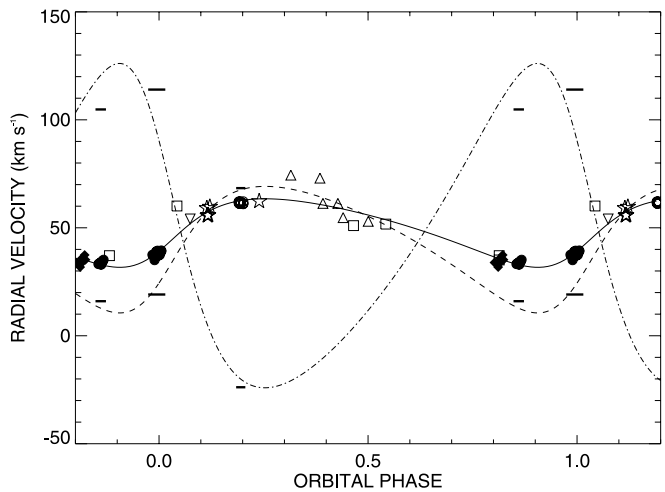

FIG. 2.—Tentative radial velocity curve (*solid line*) for HD 54662 for a period of 558 days. The measured radial velocities are indicated by filled circles (2000), filled diamonds (2006), squares (Stickland & Lloyd 2001), open circles (Fullerton 1990), stars (Garmany et al. 1980), inverted triangles (Conti et al. 1977), and triangles (Plaskett 1924). Expanded horizontal bars are plotted to show the radial velocities derived from fitting the composite line profile from the average spectra for three observational epochs (§ 5). The dashed and dot-dashed lines are the radial velocity curves to these time-averaged points for the primary and secondary star, respectively. The uncertainties in individual measurements are generally smaller than the size of the symbols.

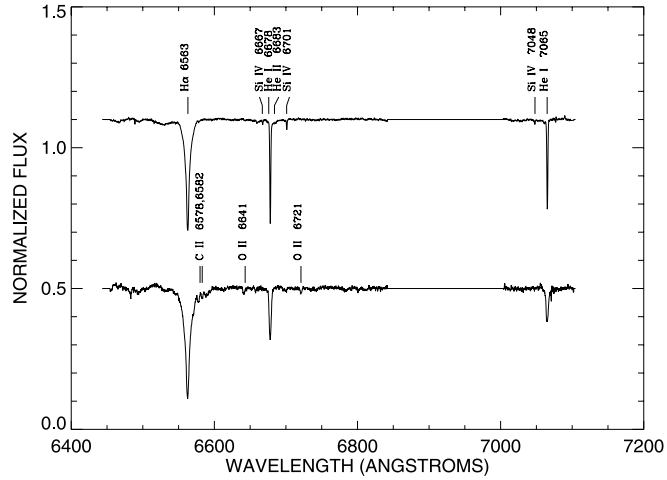

FIG. 3.—Tomographic reconstruction of the spectra of HD 37366 based on the 30 red spectra obtained in 2000. This plot shows the primary (*top*) and the secondary (*bottom*) spectrum, as well as absorption-line identifications (*vertical marks*). The atmospheric lines in the region of 6850–7000 Å are replaced with the continuum.

TABLE 5
STELLAR PARAMETERS FOR HD 37366

Parameter	Value
$V_1 \sin i$ (km s^{-1})	30 ± 10
$V_2 \sin i$ (km s^{-1})	100 ± 10
$T_{\rm eff,\,1}$ (kK)	33 ± 1
$T_{\rm eff,\,2}$ (kK)	30 ± 1
$\log g_1$ (cgs)	4.0 ± 0.1
$\log g_2$ (cgs)	4.5 ± 0.2
F_2/F_1	0.35 ± 0.05
ΔM_V	1.1 ± 0.1

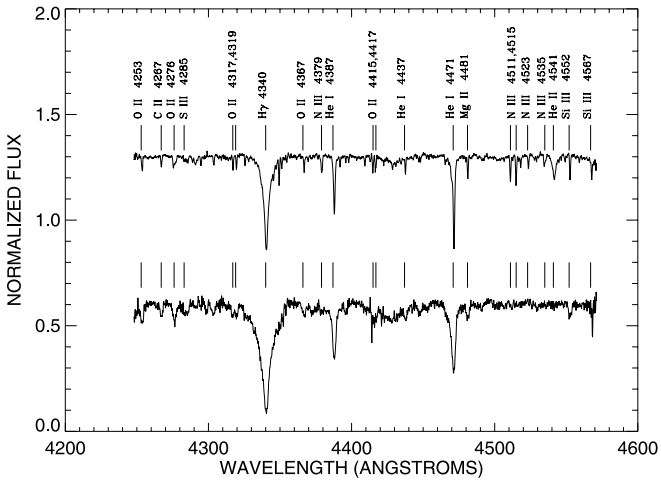

FIG. 4.—Tomographic reconstruction of the spectra of HD 37366 based on five blue spectra from runs in 2005 and 2006. Plot same as in Fig. 3.

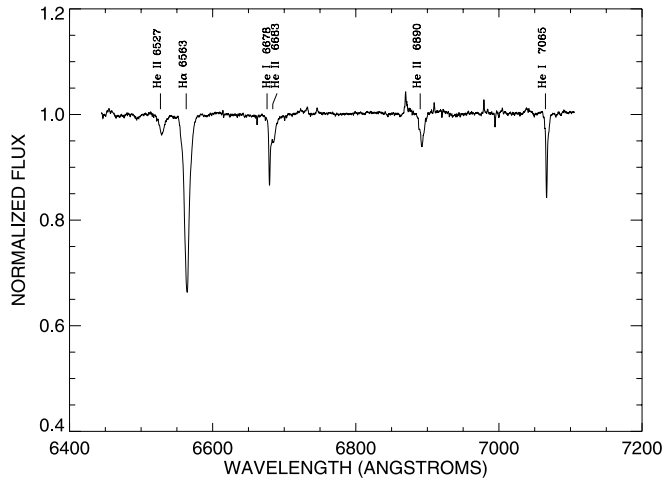

FIG. 5.—Mean spectrum of HD 54662 from our observations. Line identifications are marked by vertical lines.

parameters, and the results were later checked with the reconstructed blue spectra, which include Hγ as well as other lines from heavier elements. The small $V \sin i$ estimate we derive for the primary agrees with the *IUE* measurements from Howarth et al. (1997) and Stickland & Lloyd (2001), and is much smaller than the value for the broader lined secondary. The primary's temperature is somewhat larger than the $T_{\rm eff} = 29.0 \pm 1.8$ kK estimate by Grigsby et al. (1992), but the gravities agree exactly. Our results for $T_{\rm eff}$ and $\log g$ using the TLUSTY code are expected to be more reliable than the previous models used in Grigsby et al. (1992), which used the PAM code (Anderson 1985) that only includes nine elements and many fewer metal lines than does TLUSTY.

The reconstructions from the five high-resolution blue spectra are presented in Figure 4 along with identifications of absorption lines. The secondary spectrum (*bottom*) has lower S/N, but even with only five spectra the tomography algorithm was able extract its spectrum. It is again apparent that the lines of the secondary are much broader than those of the primary. Note also the absence of the He II λ4541 line in the secondary's spectrum, reinforcing our conclusion that the secondary is the cooler of the two stars. Based on the secondary's cooler temperature and high surface gravity, we estimate that it is a B0–1 V star. Note that the magnitude difference we derive is larger than expected for main-sequence stars separated by only a subtype or so (Martins et al. 2005), so it is possible that the primary is a somewhat evolved, more luminous star, and/or the companion is a very young star close to the zero-age main sequence (ZAMS). It is interesting to note that the high $M_1 \sin^3 i$ and $M_2 \sin^3 i$ values from the orbital solution suggest that the inclination is large, $i = 60°$–$90°$. However, *Hipparcos* photometry plotted with the period from our spectroscopic orbital solution shows no evidence of eclipses.

5. STELLAR PARAMETERS FOR HD 54662 FROM COMPOSITE PROFILE FITS

Radial velocities measured for HD 54662 were used to create mean spectra for our observations made in 2000 (Fig. 5) and for those made by Fullerton (1990) in 1986. Figure 6 shows an expanded view of the regions surrounding the He I profiles for two epochs of observation. We see that the secondary component appeared blueshifted during the 1986 run (*left*) and redshifted in recent spectra (*right*).

We made preliminary two-component fits of the blended He I lines (λ5876 for the spectra obtained by Fullerton 1990 and λ7065 for this work) using TLUSTY/SYNSPEC models. We used the temperature and gravity calibrations of Martins et al. (2005) to select parameters for the composite model profiles to fit our observations. Our model spectra for the primary star are based on an assumed type of O6.5 V (Walborn 1972). We constructed model spectra for the secondary for spectral subtypes of O7 V–O9.5 V. Next, we compared our observed mean line profiles to these models applying the appropriate flux ratio (from ΔM_V in Martins et al. 2005) for each spectral component in the shifted, combined line profiles. In each trial for a given secondary spectral type, the only variables were the component radial velocities and the secondary's projected rotational velocity $V_2 \sin i$ (we assumed $V_1 \sin i = 70$ km s^{-1}; Conti & Ebbets 1977). Our best match for the secondary was made with an O9 V subtype and $V_2 \sin i = 110 \pm 10$ km s^{-1}, which yields a flux ratio of $F_2/F_1 = 0.51$. Our fits of He I λ7065 required us to make small and equal adjustments to the model line depths. The resulting fits are shown in Figure 6. We caution that an uncertainty in $V_2 \sin i$ has a large effect on the best-fit line shifts and flux ratio results.

The wavelength shifts made to fit these composite line profiles provide us with average velocities for the primary and secondary components for each observing run. Assuming that the true anomaly ν and the longitude of periastron ω are known from the preliminary orbital fit (Table 4), we may estimate the systematic velocity γ and semiamplitude K by making a least-squares, linear fit of these three velocities using

$$V_r = \gamma_{1,2} \pm K_{1,2}[\cos(\nu + \omega) + e \cos \omega]. \quad (2)$$

This solution gives semiamplitudes of $K_1 = 29 \pm 4$ and $K_2 = 75 \pm 7$ km s^{-1} and systemic velocities of $\gamma_1 = 45 \pm 3$ and $\gamma_2 = 40 \pm 6$ km s^{-1}. This estimate of the secondary radial velocity curve also allows us to compute the component minimum masses of the system, $M_1 \sin^3 i \approx 41.5 \pm 7.6\ M_\odot$ and $M_2 \sin^3 i \approx 16.0 \pm 3.4\ M_\odot$. The radial velocity curves for these solutions for the primary (*dashed line*) and secondary (*dot-dashed line*) are also plotted in Figure 2, along with the time-averaged radial velocities from the two-component fits. This analysis of the line blending problem clearly illustrates how the presence of the blended secondary spectrum skews the velocity measurements

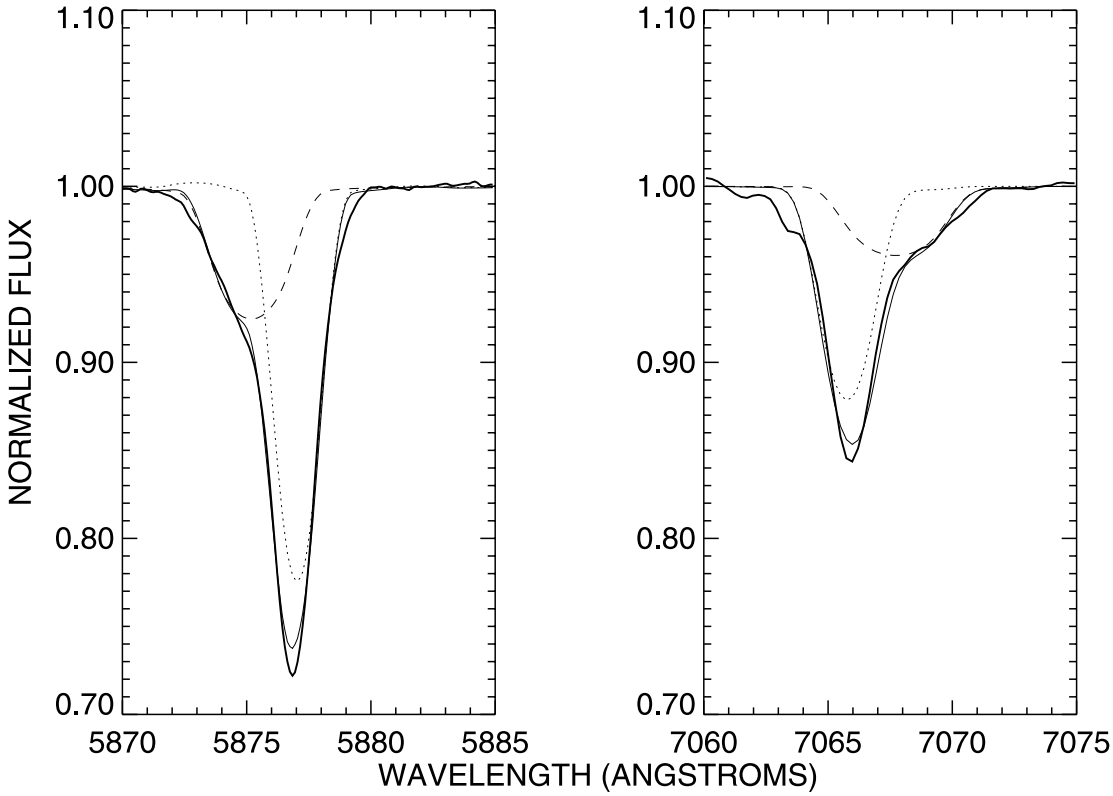

FIG. 6.—Mean line profiles of HD 54662 for He I λ5876 (*left*; Fullerton 1990) and He I λ7065 (*right*; this work). The observations are plotted as thick lines, the combined model fit as thin lines, and the individual component profiles as dotted and dashed lines for the primary and secondary, respectively.

for the primary (Table 3) toward the system's center of mass, resulting in a semiamplitude (Table 4) that is approximately a factor of 2 smaller than the actual value.

6. DISCUSSION

One of the motivations for this study was to find long-period binaries that may be resolved by optical long-baseline interferometry. The CHARA Array, for example, can resolve binaries with angular separations as small as 1 mas (ten Brummelaar et al. 2005). To determine the angular separation of the binaries' components, we reestimated their distances by fitting their observed spectral energy distribution (SED) with a model SED to find the angular stellar diameters that we then compared with stellar radii estimates for their spectral classifications. For each binary, the model temperatures, gravities, and flux ratios were applied to create a combined model flux distribution over a range of 1200–30000 Å. The galactic extinction curve from Fitzpatrick (1999) was then applied to the model SED to fit the observed photometry for each target. The observed SED includes ultraviolet fluxes (*IUE*; TD-1; Thompson et al. 1978) and *UBV* (Neckel et al. 1980), *uvby* (Hauck & Mermilliod 1998), and 2MASS (Two Micron All Sky Survey) *JHK* infrared magnitudes (Skrutskie et al. 2006; Cutri et al. 2003), all of which were transformed into calibrated flux measurements (Colina et al. 1996; Gray 1998; Cohen et al. 2003). The best-fit parameters for reddening $E(B-V)$, ratio of total-to-selective extinction R, and the limb-darkened angular diameter for the primary θ_{LD} (from the flux normalization) are listed in Table 6. Figures 7 and 8 show the SED plots of these best fits for HD 37366 and HD 54662, respectively.

TABLE 6
SED PARAMETERS

Parameter	HD 37366	HD 54662
Primary type	O9.5 V[a]	O6.5 V[a]
Secondary type	B0–1 V	O9 V
$E(B-V)$ (mag)	0.39 ± 0.01	0.32 ± 0.01
R_V (mag)	3.59 ± 0.01	2.82 ± 0.01
θ_{LD} (μas)[b]	48.4 ± 3.0	72.7 ± 3.4
d (kpc)	1.38–1.92	1.23–1.53
$\rho_{\max}$ (mas)	0.4–0.5	3.7–4.7

[a] Walborn (1972, 1973).
[b] Primary.

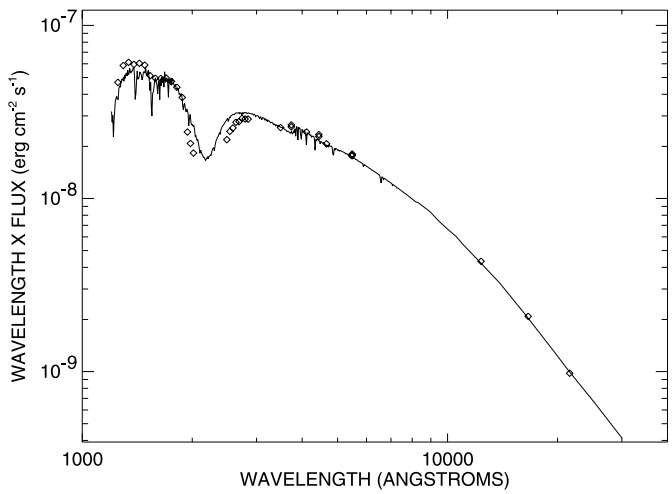

FIG. 7.—Best-fit SED for HD 37366. The solid line indicates the combined model flux for the binary, and the diamonds represent the photometric observations (described in the text).

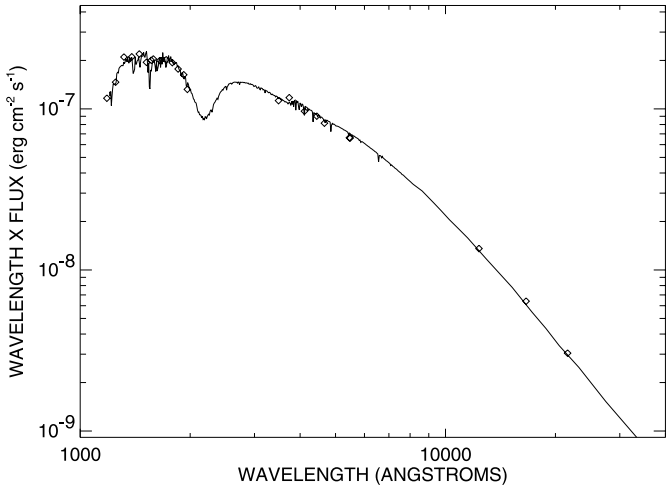

FIG. 8.—Same as Fig. 7, but for HD 54662.

We then compared the expected theoretical radii for the primary stars, based on their spectral classifications as main-sequence stars (Martins et al. 2005), with the angular sizes to obtain distances of 1.38 and 1.23 kpc for HD 37366 and HD 54662, respectively (Table 6). These estimates are consistent with the accepted distances to their home associations (Humphreys 1978). The distance ranges given in Table 6 reflect the change in stellar radius between ZAMS luminosity class V and giant luminosity class III. The midpoint increase in size is $\triangle R \approx 3\ R_{\odot}$ for our stars, and we adopted this difference to estimate the associated range in distance. Errors will also result from the spread in radius for each spectral subtype bin, but this is quite small ($\pm 0.4\ R_{\odot}$) compared to the luminosity range. The error in θ_{LD} from the SED fit contributes only $\approx$1% in the distance error budget.

The binary semimajor axis a was found using Kepler's third law, the derived orbital period, and the stellar mass calibrations from Martins et al. (2005; for O stars) and Harmanec (1988; for B stars). The results for the maximum angular separation $\rho_{\max}$ for the projected elliptical orbit are also presented in Table 6, where we give the range in $\rho_{\max}$ associated with the range in distance. These separations are too small for speckle resolution ($\rho > 0.035''$ for $\triangle m < 3.0$), but they are close to or above the limits of long-baseline interferometry. The HD 54662 binary system in particular may prove to be an important target for mass determination by interferometry.

We thank Daryl Willmarth, Paul Rybski, Eric Phillips, Travis Fischer, and the KPNO staff for their assistance in making these observations possible. This material is based on work supported by the National Science Foundation (NSF) under grants AST 05-06573 and AST 06-06861. C. T. B.'s research is partially supported by a Natural Sciences and Engineering Research Council of Canada (NSERC) Discovery Grant. A. W. F. held an NSERC Post graduate scholarship during the course of this work. Some of the data presented in this paper were obtained from the Multimission Archive at the Space Telescope Science Institute (MAST). STScI is operated by the Association of Universities for Research in Astronomy, Inc., under National Aeronautics and Space Administration (NASA) contract NAS5-26555. Support for MAST for non-*HST* data is provided by the NASA Office of Space Science via grant NAG5-7584 and by other grants and contracts. This publication makes use of data products from the Two Micron All Sky Survey (2MASS), which is a joint project of the University of Massachusetts and the Infrared Processing and Analysis Center/California Institute of Technology, funded by NASA and NSF.

REFERENCES

Anderson, L. S. 1985, ApJ, 298, 848
Bagnuolo, W. G., Jr., Gies, D. R., Hahula, M. E., Wiemker, R., & Wiggs, M. S. 1994, ApJ, 423, 446
Cohen, M., Wheaton, W. A., & Megeath, S. T. 2003, AJ, 126, 1090
Colina, L., Bohlin, R., & Castelli, F. 1996, *HST* Instrument Science Report CAL/SCS-008 (Baltimore: STScI)
Conti, P. S. 1974, ApJ, 187, 539
Conti, P. S., & Ebbets, D. 1977, ApJ, 213, 438
Conti, P. S., Leep, E. M., & Lorre, J. J. 1977, ApJ, 214, 759
Cutri, R. M., et al. 2003, The 2MASS All Sky Catalog of Point Sources (Pasadena: IPAC)
De Becker, M., Rauw, G., Manfroid, J., & Eenens, P. 2006, A&A, 456, 1121
Fitzpatrick, E. L. 1999, PASP, 111, 63
Fullerton, A. W. 1990, Ph.D. thesis, Univ. Toronto
Garmany, C. D., Conti, P. S., & Massey, P. 1980, ApJ, 242, 1063
Garmany, C. D., & Massey, P. 1981, PASP, 93, 500
Gies, D. R. 2003, in IAU Symp. 212, A Massive Star Odyssey: From Main Sequence to Supernova, ed. K. van der Hucht, A. Herrero, & C. Esteban (San Francisco: ASP), 91
Gies, D. R., Penny, L. R., Mayer, P., Drechsel, H., & Lorenz, R. 2002, ApJ, 574, 957
Gies, D. R., et al. 1997, ApJ, 475, L49
Gray, R. O. 1998, AJ, 116, 482
Grigsby, J. A., Morrison, N. D., & Anderson, L. S. 1992, ApJS, 78, 205
Harmanec, P. 1988, Bull. Astron. Inst. Czechoslovakia, 39, 329
Hauck, B., & Mermilliod, M. 1998, A&AS, 129, 431
Howarth, I. D., Siebert, K. W., Hussain, G. A. J., & Prinja, R. K. 1997, MNRAS, 284, 265
Hubeny, I. 1988, Comput. Phys. Commun., 52, 103
Hubeny, I., Heap, S. R., & Lanz, T. 1998, in ASP Conf. Ser. 131, Boulder-Munich II: Properties of Hot Luminous Stars, ed. I. D. Howarth (San Francisco: ASP), 108
Hubeny, I., & Lanz, T. 1995, ApJ, 439, 875
Humphreys, R. M. 1978, ApJS, 38, 309
Lanz, T., & Hubeny, I. 2003, ApJS, 146, 417
Martins, F., Schaerer, D., & Hillier, D. J. 2005, A&A, 436, 1049
Mason, B. D., Gies, D. R., Hartkopf, W. I., Bagnuolo, W. G., Jr., ten Brummelaar, T., & McAlister, H. A. 1998, AJ, 115, 821
McKibben, W. P., et al. 1998, PASP, 110, 900
Morbey, C. L., & Brosterhus, E. B. 1974, PASP, 86, 455
Neckel, T., Klare, G., & Sarcander, M. 1980, A&AS, 42, 251
Penny, L. R., Gies, D. R., & Bagnuolo, W. G., Jr. 1999, ApJ, 518, 450
Perryman, M. A. C., et al. 1997, The *Hipparcos* and Tycho Catalogues (ESA SP-1200; Noordwijk: ESA)
Petrie, R. M., & Pearce, J. A. 1961, Publ. Dom. Astrophys. Obs. Victoria, 12, 1
Plaskett, J. S. 1924, Publ. Dom. Astrophys. Obs. Victoria, 2, 285
Roberts, D. H., Lehár, J., & Dreher, J. W. 1987, AJ, 93, 968
Skrutskie, M. F., et al. 2006, AJ, 131, 1163
Stickland, D. J., & Lloyd, C. 2001, Observatory, 121, 1
ten Brummelaar, T. A., et al. 2005, ApJ, 628, 453
Thompson, G. I., Nandy, K., Jamar, C., Monfils, A., Houziaux, L., Carnochan, D. J., & Wilson, R. 1978, Catalogue of Stellar Ultraviolet Fluxes: A Compilation of Absolute Stellar Fluxes Measured by the Sky Survey Telescope (S2/68) aboard the ESRO Satellite TD-1 (London: Science Research Council)
Walborn, N. R. 1972, AJ, 77, 312
———. 1973, AJ, 78, 1067
Young, R. K. 1942, Publ. David Dunlap Obs., 1, 251